A *Burkholderia pseudomallei* Toxin Inhibits Helicase Activity of Translation Factor eIF4A

Abimael Cruz[1,*], Guillaume M. Hautbergue[1,*], Peter J. Artymiuk[1], Patrick J. Baker[1], Monika Bokori-Brown[2], Chung-Te Chang[1], Mark J. Dickman[3], Angela Essex-Lopresti[4], Sarah V. Harding[4], Nor Muhammad Mahadi[5], Laura E. Marshall[4], George W. Mobbs[1], Rahmah Mohamed[5,6], Sheila Nathan[5,6], Sarah A. Ngugi[4], Catherine Ong[7], Wen Fong Ooi[8], Lynda J. Partridge[1], Helen L. Phillips[3],M. Firdaus Raih[6], Sergei Ruzhenikov[1], Mitali Sarkar-Tyson[4], Svetlana E. Sedelnikova[1], Sophie J. Smither[4], Patrick Tan[8], Richard W. Titball[2], Stuart A. Wilson[1,#], David W. Rice[1,#]

[1]Krebs Institute, Department of Molecular Biology and Biotechnology, University of Sheffield, Sheffield S10 2TN, UK

[2]College of Life and Environmental Sciences, University of Exeter, Stocker Road, Exeter, Devon UK, EX4 4QD.

[3]ChELSI Institute, Department of Chemical and Biological Engineering, University of Sheffield, The Sheffield Bioincubator, 40 Leavygreave Road, Sheffield, S3 7RD

[4]Defence Science and Technology Laboratory, Porton Down, Salisbury, Wiltshire, SP4 OJQ, UK

[5]Malaysia Genome Institute, Jalan Bangi, 43000 Kajang, Selangor DE, Malaysia

[6]School of Biosciences & Biotechnology, Faculty of Science & Technology, Universiti Kebangsaan Malaysia, 43600 Bangi, Selangor DE, Malaysia

[7]Defence Medical & Environmental Research Institute, DSO National Laboratories, 27 Medical Drive, 117510, Singapore.

[8]Genome Institute of Singapore, 60 Biopolis Street, 138672, Singapore.

[*] These authors contributed equally.

[#] To whom correspondence should be addressed.

E-mail:stuart.wilson@sheffield.ac.uk or D.Rice@sheffield.ac.uk

Abstract

The structure of BPSL1549, a protein of unknown function from *Burkholderia pseudomallei* reveals a similarity to *E. coli* cytotoxic necrotizing factor 1. We found that BPSL1549 acted as a potent cytotoxin against eukaryotic cells and was lethal when administered to mice. Expression levels of *bpsl1549* correlate with conditions expected to promote or suppress pathogenicity. BPSL1549 promotes deamidation of Gln^{339} of the translation initiation factor eIF4A, abolishing its helicase activity and inhibiting translation. We propose to name BPSL1549 *Burkholderia* Lethal Factor 1 (BLF1).

The bacterium *Burkholderia pseudomallei* is the causative agent of melioidosis (*1*) and, in endemic areas including Southeast Asia, can be isolated from moist soil and stagnant water. *B. pseudomallei* infects many tissue, causing subclinical infections, acute septicaemia and sub-acute and chronic disease. The pathogen has the ability to remain latent in a host for decades (*2*) and infections in troops serving in endemic areas has resulted in the pathogen being referred to by the nickname, the “Vietnam Time Bomb” (*3*). There is no vaccine and the organism is multidrug resistant complicating treatment. The molecular mechanisms that underlie disease are largely unknown. To address this, a programme of structure determination on proteins of unknown function from *B. pseudomallei* has been initiated.

The structure of BPSL1549, a 23 kDa protein of unknown function, was determined at 1.04 Å resolution (Table S1, Fig. S1A). The fold consists of a sandwich of two curved mixed beta sheets decorated on the outside by alpha helices and loops (Fig 1A) and was similar to the catalytic domain of *E. coli* cytotoxic necrotizing factor 1 (CNF1-C) (*4*) . Eleven strands of the BPSL1549 beta sandwich have identical sequence order and direction to those of CNF1-C, with an rmsd of 3.9 Å for 170 superposed α-carbon atoms (Fig. 1B). However, on the peripheries of the structures there are differences in both the extensions to the β-strands and the helices and loops, with only one helix in common.

CNF1-C inactivates Rho GTPases by deamidation of a glutamine necessary for GTPase hydrolysis, thereby affecting actin cytoskeleton assembly (*5*). CNF1-C and BPSL1549 showed virtually no sequence identity, except at the active sites where the LSGC motif of CNF1-C was conserved in BPSL1549 (Fig. S1B,C). The cysteine of this motif, Cys^{866}/ Cys^{94} in CNF1-C and BPSL1549, respectively, is the crucial nucleophile in the CNF1-C catalytic triad responsible for deamidase activity (*4*). His^{881}, the second component of the CNF1-C triad was present in BPSL1549 (as His^{106}) and superposed well (Fig. 1C). In CNF1-C the third component of the triad is a main chain carbonyl, but in BPSL1549 the OG1 of Thr^{88} hydrogen bonds to the histidine. A structurally conserved tyrosine (Tyr^{164} in BPSL1549, Tyr^{962} in CNF1-C)

hydrogen bonds to the main chain carbonyl of the catalytic cysteine (Fig. 1C).

The conservation of key catalytic residues with CNF1-C, suggested BPSL1549 was a glutamine deamidase. However, the molecular surface around the BPSL1549 active site cavity was broader and shallower than that of CNF1-C suggesting the deamidation target was different (Fig S2). Nevertheless, the structure implied that, like CNF1-C, BPSL1549 might be cytotoxic. Intraperitoneal injection of Balb/C mice with BPSL1549 was lethal by day 14 (Supplementary online material). BPSL1549 was also toxic to J774 macrophage cells within 3 days (Fig. 2A). In contrast, growth of 3T3 cells was insensitive to BPSL1549 unless the protein delivery reagent BioPORTER was included (Fig. S3A). The differential sensitivity between macrophages and fibroblasts may reflect uptake by active macropinocytosis in macrophages, although how the toxin accesses the cytoplasm is unclear.

On the basis of the abolition of the biological activity of CNF1 when Cys^{866} is mutated to serine, a BPSL1549C94S mutant was created. In mice BPSL1549C94S was non-toxic, whereas in J774 cells some toxicity ($p < 0.05$) was observed, but only at the highest toxin concentration tested (Fig 2A). Thermal stability studies (Fig. S3B,C) together with the BPSL1549C94S structure (Table S1) confirmed that this point mutation does not disrupt the structure and that C94 is required for BPSL1549 activity.

To investigate a role for *bpsl1549* in bacterial virulence, an in-frame deletion mutant of *bpsl1549* in *B. pseudomallei* was constructed. Whilst we cannot exclude the influence of polarity effects in the *Δbpsl1549* strain, compared to the wild type strain the mutant was significantly attenuated when mice were challenged by the i.p. route (Fig. 2B). The median lethal dose of *B. pseudomallei Δbpsl1549* was 1.26×10^5 colony forming units (CFU), 100 times higher than that for the wild type *B. pseudomallei* strain K96243, consistent with a role for *bpsl1549* in virulence. Moreover, *bpsl1549* expression was highly upregulated in response to multiple virulence cues (Fig. S4).

An affinity column was used to purify BPSL1549 binding-partners from human cell extract. The major protein purified was translation initiation factor

eIF4A which was confirmed by immunoblotting (Fig. 3A). Interaction with endogenous eIF4A was verified by coimmunoprecipitation with FLAG-BPSL1549. FLAG-BPSL1549C94S precipitated more eIF4A than FLAG-BPSL1549, suggesting that release of the substrate from the toxin requires completion of deamidation (Fig. 3B).

The BPSL1549:eIF4A interaction suggested BPSL1549 might inhibit translation and its expression in human cells led to 90% or greater reduction in gene expression for two reporters. Reduced translation inhibition by BPSL1549C94S may result from binding eIF4A (Fig. 3B,C). The reporter mRNA levels were unaffected, consistent with BPSL1549 blocking translation (Fig. 3C, right panel). BPSL1549 reduced endogenous protein synthesis monitored by ^{35}S-Met/Cys incorporation at levels similar to that seen with the eIF4A inhibitor hippuristanol (*6*), whereas BPSL1549C94S did not (Fig. 3D). The ongoing translation in the presence of BPSL1549 may arise from eIF4A-independent mRNAs. To assess the impact of BPSL1549 on translation initiation we monitored the abundance of ribosomal subunits, monosomes and polysomes in cell extracts (Fig. 3E). BPSL1549 enhanced the size of the 80S peak and reduced the size of the polysome peaks with polyA binding protein (PABP) being absent in this region of the gradient. This suggested translation initiation was stalled , mirroring the situation seen with the eIF4A specific inhibitor pateamine A (*7*).

A translational block can trigger cytoplasmic stress granule formation either by an eIF2α phosphorylation-dependent or independent pathways induced by cellular stresses or by inactivation of eIF4A, 4G, 4B,4H or PABP respectively (*8*). Sodium arsenate treatment led to both stress granule formation and eIF2α phosphorylation (Fig S5). BPSL1549 expression also caused stress granule formation, but not eIF2α phosphorylation, consistent with activation of the eIF2α phosphorylation-independent pathway. BPSL1549C94S failed to trigger stress granule formation efficiently, consistent with its reduced ability to inhibit translation.

To identify the modification in eIF4A we used MS to analyse FLAG-eIF4AI purified from human cells expressing BPSL1549 (Fig. S6). MS revealed deamidation of Gln^{339} to Glu (Fig. 4A). Gln^{339} is in the C-terminal

domain of eIF4A and is the first glutamine of a conserved Gln-Gln pair lying between motifs V and VI (*9*). This loop is adjacent to the cleft between the enzyme's two domains and lies between the ATP and RNA binding sites (Fig S7) suggesting modification might inhibit eIF4A ATPase or helicase activities. In vitro, BPSL1549 deamidates eIF4A Gln^{339} with a turnover number of ~700 per minute, similar to the rate of depurination catalysed by ricin (*10*) (Fig. S8, S9). Consistent with Gln^{339} being the target residue, BPSL1549 binds less efficiently to eIF4AIQ339E, the product of the deamidation reaction (Fig. S10). Two isoforms of eIF4A (I and II) have a glutamine at position 339, whereas eIF4AIII, an exon junction complex subunit, has proline at this position and is unlikely to be a BPSL1549 substrate.

Expression of eIF4AI Q339E in vivo reduced expression of two reporters, indicating Q339E is dominant negative, whereas control mutation Q340E had no effect (Fig. 4B). Q339E had no effect on eIF4A1 ATPase activity or RNA and ATP binding (Fig. S11). However, Q339E reduced RNA helicase activity (Fig. 4C). eIF4AI mutations that uncouple the ATPase and helicase activities are known to act as inhibitors of translation (*11*). At molar ratios of 1:500 BPSL1549:eIF4A there was 47% inhibition of helicase activity indicative of enzymatic modification by BPSL1549. Whereas BPSL1549C94S only caused 15% inhibition of helicase activity at a molar ratio of 1:10 BPSL1549C94S:eIF4A, probably caused by BPSL1549C94S binding to eIF4A (Fig S12). Based on the closed conformation structure of eIF4AIII (*12*), Gln^{339} in eIF4AI would lie close to Asp^{337} and Arg^{368} and the 3' adenine ribose hydroxyl of ATP (Fig. S13). Thus, deamidation of Gln^{339} probably disrupts interaction between these residues, influencing the functions of Asp^{337}. In the Vasa RNA helicase, the structural equivalent of eIF4AI Asp^{337} is Asp^{534} and a D534A mutation uncouples ATP hydrolysis and RNA binding from the helicase activity (*13*).

We examined the impact of BPSL1549 on formation of the cap binding complex eIF4F. BPSL1549 had no impact on the levels of eIF4E, 4G1 or PABP bound, but increased the amount of eIF4A recovered (Fig. 4D), suggesting eIF4A was more stably bound within eIF4F. Endogenous eIF4A was readily exchanged with recombinant eIF4A within eiF4F when cell

extracts were pre-incubated with the control splicing factor SC35 (Fig. 4E lanes 6,7) but in cell extracts pre-incubated with BPSL1549, recombinant eIF4A did not efficiently displace endogenous eiF4A from eIF4F. Thus recycling of eIF4A, required for efficient translation (*11*),(*14*) would be impaired.

Compared to CNF1-C a major difference with BPSL1549 is the lack of the receptor binding and translocation domains, essential for cytoplasmic delivery of CNF1-C. However, the intracytoplasmic lifestyle of *B. pseudomallei* removes the need for BPSL1549 to cross the eukaryotic cell membrane, though the absence of an obvious BPSL1549 signal sequence leaves its mechanism of secretion uncertain. The demonstration that BPSL1549 is a potent inhibitor of translation suggests that it is an important weapon in the armoury of *B. pseudomallei* and we suggest renaming it *Burkholderia* Lethal Factor 1 (BLF1). The identification of structurally unrelated papain-like glutamine deamidases CHBP in *B. pseudomallei* (*15*) and PMT in *Pasteurella multocida (16)* suggests this type of chemistry may be more generally employed by pathogenic bacteria than is currently recognised.

Figure Legends

Fig. 1 Structural analysis of BPSL1549 (A) Cartoon representation of BPSL1549 with helices and strands numbered. (B) Cartoon representation showing the similarity in overall fold between BPSL1549 (blue) and CNF1-C (red). (C) Detail of superposition of BPSL1549 (pale blue) and CNF1-C (pale red) around their active sites with residues strongly conserved between the two toxins, including the critical cysteine and histidine, highlighted. Hydrogen bonds shown as dotted lines.

Fig. 2 Toxic effects of BPSL1549 (A) Effect of BPSL1549 and C94S mutant on the BALB/c J774.2 macrophage cell line after 72h. Values correspond to the means of three to seven independent experiments performed in duplicate and error bars represent S.D. Data were analysed by ANOVA and values significantly different from control (no toxin) are shown as *** $p < 0.0001$; * $p < 0.05$. Significant toxic effects were evident at concentrations down to 2.5×10^{-7} M (5.7 $\mu g.ml^{-1}$) with an EC_{50} of 2.7×10^{-7}M (6.2 $\mu g.ml^{-1}$). (B) Survival of BALB/c mice (n=6) challenged with 4.2×10^4 cfu/ml *B. pseudomallei* K96243 (●) or 5.8×10^4 cfu/ml *B. pseudomallei* K96243Δ*BPSL1549* (■) (p<0.001).

Fig. 3 BPSL1549 modifies eIF4A and blocks translation (A) SDS-PAGE analysis of human proteins eluted from a 6xHisBPSL1549 affinity column using NaCl elution buffer. The control protein was 6xHis YloQ (GTPase from *B.subtilis*). The major band was identified by mass spectrometry (MS) as eIF4A and confirmed by immunoblotting (lower panel). (B) Co-immunoprecipitation of FLAG-BPSL1549 or FLAG-BPSL1549C94S using FLAG antibody with endogenous eIF4A. FLAG-BAP (bacterial alkaline phosphatase) was used as a control. (C) Reporter gene assays 24 hours post-transfection with FLAG-BPSL1549 or FLAG-BPSL1549C94S. Enzyme assays (left panel) and qRT-PCR analysis of reporter mRNA levels (right panel). RT = reverse transcriptase. (D) ^{35}S-Met/Cys incorporation into proteins in 293T cells following transfection with control FLAG-BAP, FLAG-BPSL1549 or FLAG-BPSL1549C94S. (E) Polysome analysis of 293T cell extracts from cells transfected with FLAG or FLAG-BPSL1549 vectors. The lower panels

show immunoblots of fractions with a PABP antibody. Error bars represent the S.D. from three independent experiments.

Fig. 4. BPSL1549 inhibits eIF4AI RNA helicase activity (A) Tandem MS analysis of the deamidated peptide GIDVEQVSLVINYDLPTNR $[M+2H]^{2+}$ from eIF4A. The prominent b and y ions are highlighted. Inset shows an expanded view of the intact mass of the $[M+2H]^{2+}$ peptide (B) Reporter genes were cotransfected with wild type or Q339E eIF4AI and enzyme activities measured. FLAG-eIF4AI construct expression was confirmed by immunoblotting (lower panel). Error bars represent S.D. from three independent experiments. (C) RNA helicase assays with eIF4AI and mutants (upper panel); the lower panel shows quantification from 3 separate helicase assays with S.D. shown by error bars. Helicase activity in % = (ssRNA)/(dsRNA + ssRNA)*100. eIF4B stimulates the helicase activity of eIF4AI. UAP56 is a control RNA helicase and Magoh, a component of the exon junction complex, is a non RNA binding control. (D) Purification of eIF4F using methyl-7 GTP sepharose and Protein G sepharose as control. eIF4F components were identified by immunoblotting. (E) eIF4AI recycling assay. eIF4F was purified from extracts treated with BPSL1549 or SC35 (control) as indicated. Following purification, recombinant eIF4AI was added to eIF4F bound to methyl-7 GTP sepharose. Proteins were identified by immunoblotting. WCE = whole cell extract.

References and Notes

1. W. J. Wiersinga, T. van der Poll, N. J. White, N. P. Day, S. J. Peacock, Melioidosis: insights into the pathogenicity of Burkholderia pseudomallei. *Nat Rev Microbiol* **4**, 272 (Apr, 2006).
2. V. Ngauy, Y. Lemeshev, L. Sadkowski, G. Crawford, Cutaneous melioidosis in a man who was taken as a prisoner of war by the Japanese during World War II. *J Clin Microbiol* **43**, 970 (Feb, 2005).
3. R. Stone, Infectious disease. Racing to defuse a bacterial time bomb. *Science* **317**, 1022 (Aug 24, 2007).
4. L. Buetow, G. Flatau, K. Chiu, P. Boquet, P. Ghosh, Structure of the Rho-activating domain of Escherichia coli cytotoxic necrotizing factor 1. *Nature Structural Biology* **8**, 584 (Jul, 2001).
5. G. Flatau *et al.*, Toxin-induced activation of the G protein p21 Rho by deamidation of glutamine. *Nature* **387**, 729 (Jun 12, 1997).
6. K. A. Spriggs *et al.*, Canonical initiation factor requirements of the Myc family of internal ribosome entry segments. *Molecular and Cellular Biology* **29**, 1565 (Mar, 2009).
7. W. K. Low *et al.*, Inhibition of eukaryotic translation initiation by the marine natural product pateamine A. *Molecular Cell* **20**, 709 (Dec 9, 2005).
8. S. Mokas *et al.*, Uncoupling stress granule assembly and translation initiation inhibition. *Molecular Biology of the Cell* **20**, 2673 (Jun, 2009).
9. J. M. Caruthers, E. R. Johnson, D. B. McKay, Crystal structure of yeast initiation factor 4A, a DEAD-box RNA helicase. *Proc Natl Acad Sci U S A* **97**, 13080 (Nov 21, 2000).

10. Y. Endo, K. Tsurugi, The RNA N-glycosidase activity of ricin A-chain. The characteristics of the enzymatic activity of ricin A-chain with ribosomes and with rRNA. *J Biol Chem* **263**, 8735 (Jun 25, 1988).

11. A. Pause, N. Methot, Y. Svitkin, W. C. Merrick, N. Sonenberg, Dominant negative mutants of mammalian translation initiation factor eIF-4A define a critical role for eIF-4F in cap-dependent and cap-independent initiation of translation. *EMBO J* **13**, 1205 (Mar 1, 1994).

12. C. B. Andersen *et al.*, Structure of the exon junction core complex with a trapped DEAD-box ATPase bound to RNA. *Science* **313**, 1968 (Sep 29, 2006).

13. T. Sengoku, O. Nureki, A. Nakamura, S. Kobayashi, S. Yokoyama, Structural basis for RNA unwinding by the DEAD-box protein Drosophila Vasa. *Cell* **125**, 287 (Apr 21, 2006).

14. A. Marintchev *et al.*, Topology and regulation of the human eIF4A/4G/4H helicase complex in translation initiation. *Cell* **136**, 447 (Feb 6, 2009).

15. J. X. Cui *et al.*, Glutamine deamidation and dysfunction of ubiquitin/NEDD8 induced by a bacterial effector family. *Science* **329**, 1215.

16. J. H. Orth *et al.*, Pasteurella multocida toxin activation of heterotrimeric G proteins by deamidation. *Proc Natl Acad Sci U S A* **106**, 7179 (Apr 28, 2009).

Acknowledgements:

We thank S. Morley for providing translation factor antibodies, C.Hellen for the eIF4B vector, A. Goldman and M. Ashe for helpful suggestions, F. Salguero (VLA) and C. Taylor (Dstl) for histopathology analysis and Defence Science Organisation Laboratories, Singapore for human sera. SW and MJD acknowledge BBSRC support. RM, SN, NMM, MFR and DWR acknowledge Ministry of Science, Technology & Innovation, Government of Malaysia grant [07-05-16-MGI-GMB08] support and the British Council PMI-2 Initiative. AC thanks CONACYT for scholarship funding. MS-T acknowledges Ministry of Defence (UK) support. MJD acknowledges EPSRC support. RT acknowledges Wellcome Trust support [grant WT085162AIA]. We acknowledge ESRF and Diamond Synchrotron for beamtime and thank C. Mueller-Dieckmann and R. Flaig for assistance with stations ID29 and I04. Atomic coordinates and structure factors have been deposited in the Protein Databank (PDB) under accession codes XXXX and XXXX.

SOM content:

SOM references

References

17. K. Mack, R. W. Titball, The detection of insertion sequences within the human pathogen Burkholderia pseudomallei which have been identified previously in Burkholderia cepacia. *FEMS Microbiol Lett* **162**, 69 (May 1, 1998).

18. S. V. Harding *et al.*, The identification of surface proteins of Burkholderia pseudomallei. *Vaccine* **25**, 2664 (Mar 30, 2007).

19. J. L. Gardy *et al.*, PSORTb v.2.0: expanded prediction of bacterial protein subcellular localization and insights gained from comparative proteome analysis. *Bioinformatics* **21**, 617 (Mar 1, 2005).

20. J. D. Bendtsen, H. Nielsen, G. von Heijne, S. Brunak, Improved prediction of signal peptides: SignalP 3.0. *J Mol Biol* **340**, 783 (Jul 16, 2004).

21. G. M. Sheldrick, Experimental phasing with SHELXC/D/E: combining chain tracing with density modification. *Acta Crystallogr D Biol Crystallogr* **66**, 479 (Apr, 2010).

22. G. M. Sheldrick, A short history of SHELX. *Acta Crystallogr A* **64**, 112 (Jan, 2008).

23. H. M. Grindley, P. J. Artymiuk, D. W. Rice, P. Willett, identification of tertiary structure resemblance in proteins using a maximal common subgraph isomorphism algorithm. *Journal of Molecular Biology* **229**, 707 (Feb, 1993).

24. L. Holm, S. Kaariainen, P. Rosenstrom, A. Schenkel, Searching protein structure databases with DaliLite v.3. *Bioinformatics* **24**, 2780 (Dec, 2008).

25. H. M. Berman *et al.*, The Protein Data Bank. *Nucleic Acids Research* **28**, 235 (Jan, 2000).

26. Chen *et al.*, MolProbity: all-atom structure validation for macromolecular crystallography. Acta Crystallographica D **66**, 12 (2010)

27. P. Skehan *et al.*, New colorimetric cytotoxicity assay for anticancer-drug screening. *J Natl Cancer Inst* **82**, 1107 (Jul 4, 1990).

28. D. L. Milton, R. O'Toole, P. Horstedt, H. Wolf-Watz, Flagellin A is essential for the virulence of Vibrio anguillarum. *J Bacteriol* **178**, 1310 (Mar, 1996).

29. M. Sarkar-Tyson *et al.*, Polysaccharides and virulence of Burkholderia pseudomallei. *J Med Microbiol* **56**, 1005 (Aug, 2007).

30. C. A. Logue, I. R. Peak, I. R. Beacham, Facile construction of unmarked deletion mutants in Burkholderia pseudomallei using sacB counter-selection in sucrose-resistant and sucrose-sensitive isolates. *J Microbiol Methods* **76**, 320 (Mar, 2009).

31. L. J. Reed, H. Muench, A simple method of estimating fifty percent endpoints. *American Journal of Hygiene* **27**, 493 (1938).

32. T. Nandi *et al.*, A genomic survey of positive selection in Burkholderia pseudomallei provides insights into the evolution of accidental virulence. *PLoS Pathog* **6**, e1000845 (Apr, 2010).

33. C. Ong *et al.*, Patterns of large-scale genomic variation in virulent and avirulent Burkholderia species. *Genome Res* **14**, 2295 (Nov, 2004).

34. J. H. Chang *et al.*, Crystal structure of the eIF4A-PDCD4 complex. *Proc Natl Acad Sci U S A* **106**, 3148 (Mar 3, 2009).

35. H. Shi, O. Cordin, C. M. Minder, P. Linder, R. M. Xu, Crystal structure of the human ATP-dependent splicing and export factor UAP56. *Proc Natl Acad Sci U S A* **101**, 17628 (Dec 21, 2004).

36. K. M. Chan, D. Delfert, K. D. Junger, A direct colorimetric assay for Ca2+ -stimulated ATPase activity. *Anal Biochem* **157**, 375 (Sep, 1986).

37. M. P. Stevens *et al.*, Attenuated virulence and protective efficacy of a Burkholderia pseudomallei bsa type III secretion mutant in murine models of melioidosis. *Microbiology* **150**, 2669 (Aug, 2004).

38. G. Shalom, J. G. Shaw, M. S. Thomas, In vivo expression technology identifies a type VI secretion system locus in Burkholderia pseudomallei that is induced upon invasion of macrophages. *Microbiology* **153**, 2689 (Aug, 2007)

Fig 1

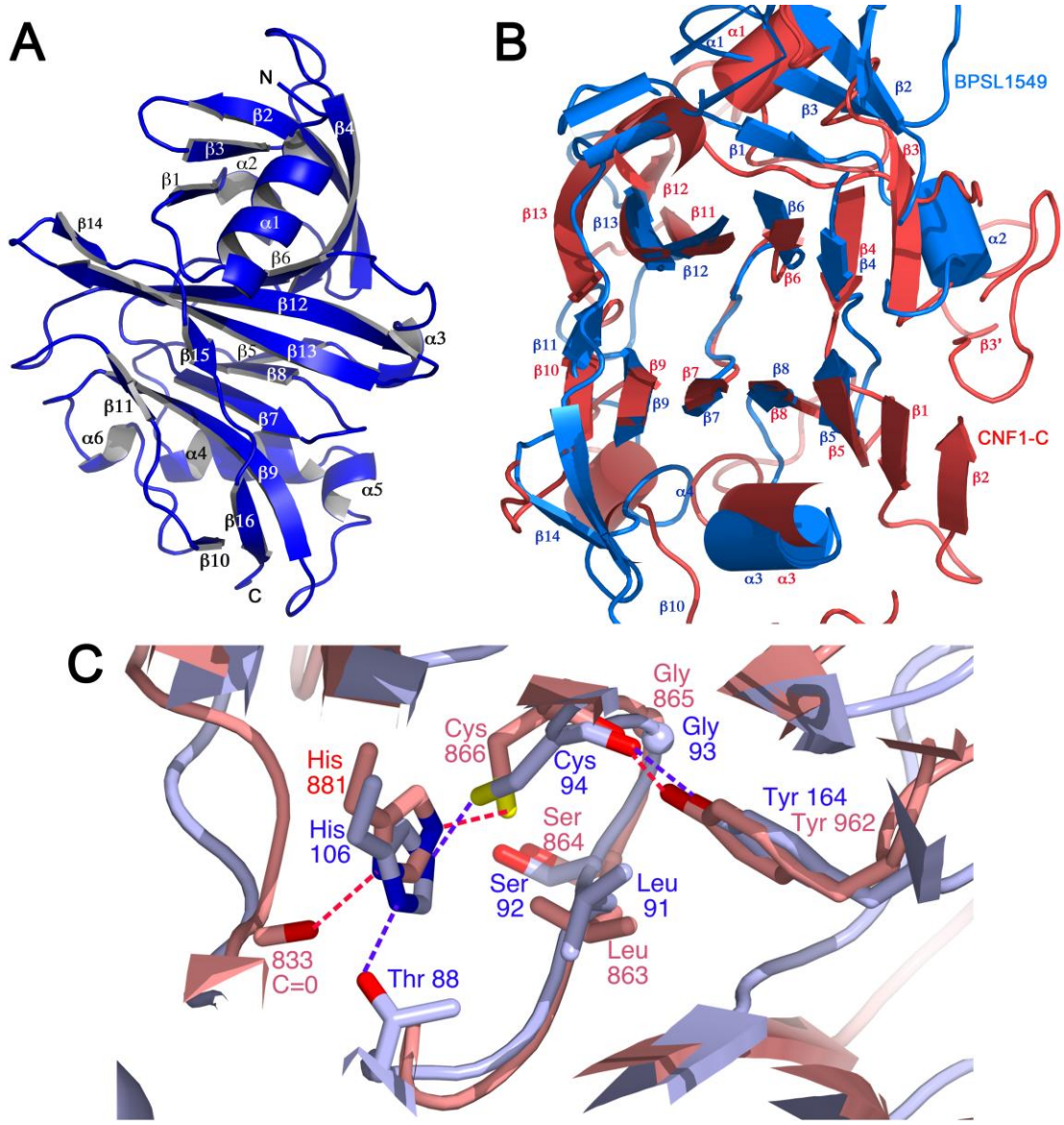
A
N
β2
β4
β3
α2
β1
β14
α1
β6
β12
α3
β15
β5
β13
β8
β11
β7
α6
α4
β9
α5
β16
β10
C
B
α1
β2
BPSL1549
β3
β1
β3
β12
β13
β11
β6
β13
β12
β4
β4
α2
β6
β3'
β11
β10
β9
β7
β8
β9
β7
β8
β1
β5
β5
CNF1-C
β2
α4
β14
α3
α3
β10
C
Gly
865
Gly
93
Cys
866
Cys
94
His
881
His
106
Ser
864
Tyr 164
Tyr 962
Ser
92
Leu
91
Leu
863
833
C=0
Thr 88

A

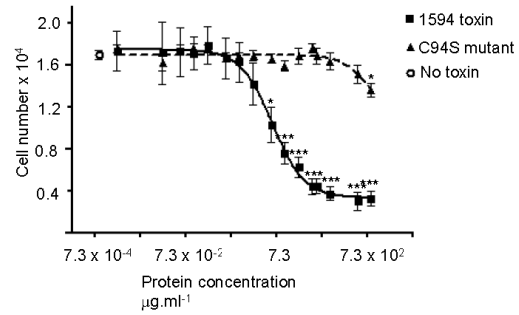
2.0
1.6
1.2
0.8
0.4
Cell number x 10⁴
7.3 x 10⁻⁴
7.3 x 10⁻²
7.3
7.3 x 10²
Protein concentration
µg.ml⁻¹
1594 toxin
C94S mutant
No toxin

B

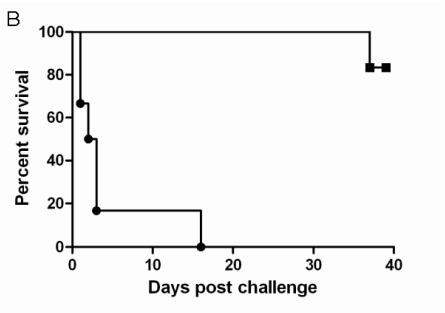
100
80
60
40
20
0
Percent survival
0
10
20
30
40
Days post challenge

Fig. 2

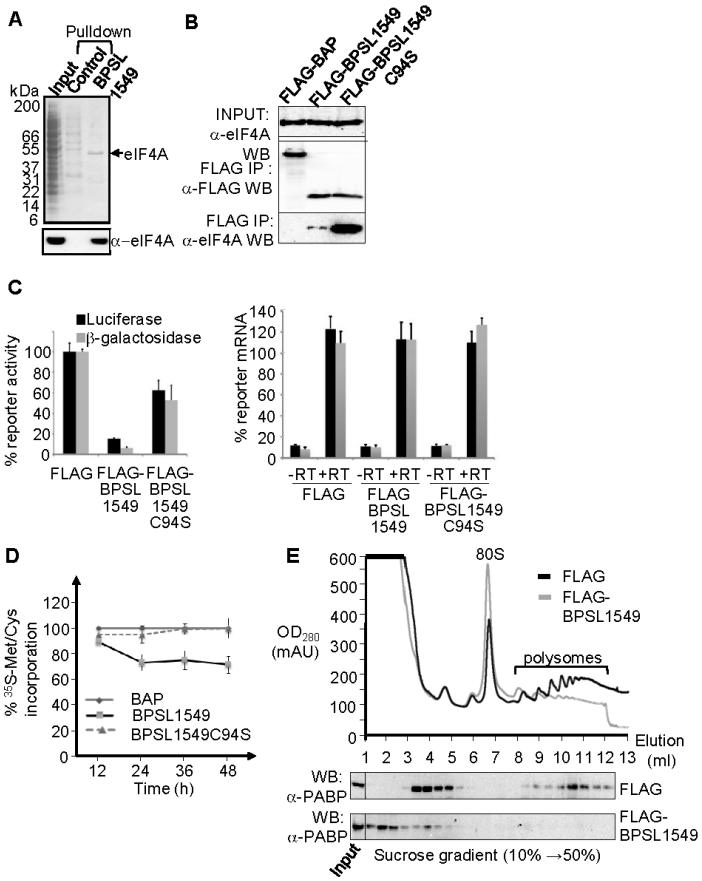
A
Pulldown
Input
Control
BPSL 1549
kDa
200
66
55
37
31
22
14.4
6
eIF4A
α–eIF4A
B
FLAG-BAP
FLAG-BPSL1549
FLAG-BPSL1549 C94S
INPUT:
α-eIF4A
WB
FLAG IP :
α-FLAG WB
FLAG IP:
α-eIF4A WB
C
Luciferase
β-galactosidase
% reporter activity
FLAG
FLAG-BPSL 1549
FLAG-BPSL 1549 C94S
% reporter mRNA
-RT +RT
FLAG
FLAG BPSL 1549
FLAG-BPSL1549 C94S
D
% 35S-Met/Cys incorporation
BAP
BPSL1549
BPSL1549C94S
Time (h)
E
80S
FLAG
FLAG-BPSL1549
OD280 (mAU)
polysomes
Elution (ml)
WB: α-PABP
FLAG
FLAG-BPSL1549
Input
Sucrose gradient (10% →50%)

Fig. 3

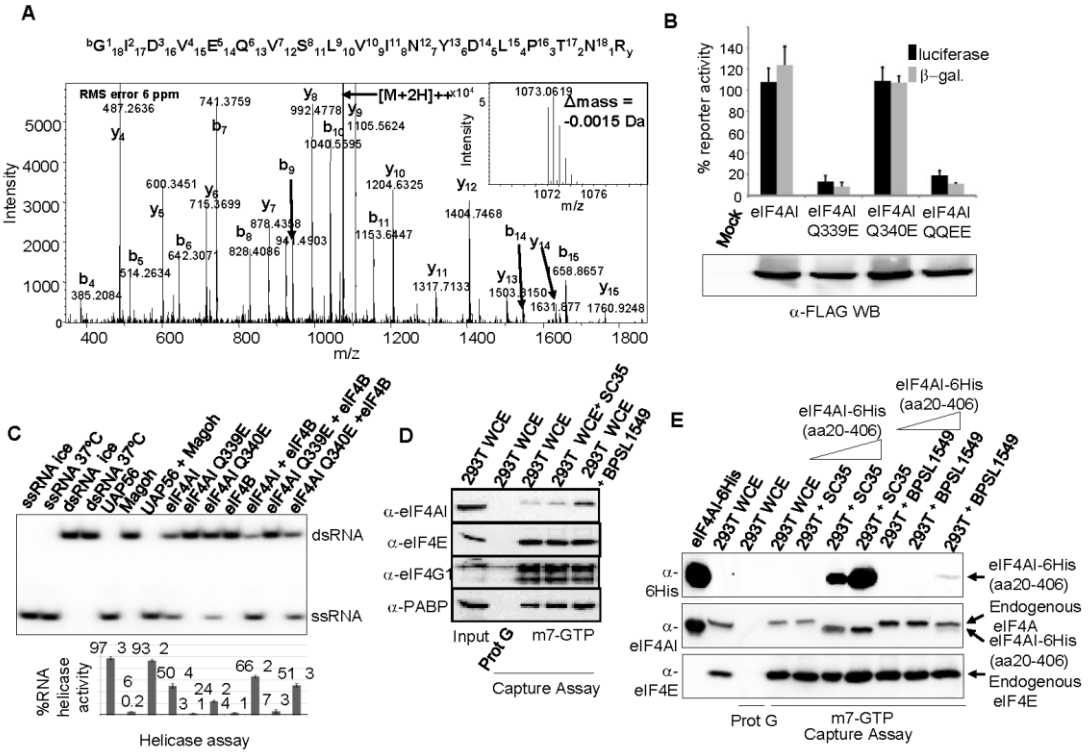
A
B
C
D
E
RMS error 6 ppm
[M+2H]++
Δmass = -0.0015 Da
Intensity
m/z
% reporter activity
luciferase
β–gal.
Mock
eIF4AI
eIF4AI Q339E
eIF4AI Q340E
eIF4AI QQEE
α-FLAG WB
ssRNA ice
ssRNA 37°C
dsRNA ice
dsRNA 37°C
UAP56
Magoh
UAP56 + Magoh
eIF4AI
eIF4AI Q339E
eIF4AI Q340E
eIF4B
eIF4AI + eIF4B
eIF4AI Q339E + eIF4B
eIF4AI Q340E +eIF4B
dsRNA
ssRNA
%RNA helicase activity
Helicase assay
293T WCE
293T WCE + SC35
293T WCE + BPSL1549
α-eIF4AI
α-eIF4E
α-eIF4G1
α-PABP
Input
Prot G
m7-GTP
Capture Assay
eIF4AI-6His (aa20-406)
α-6His
α-eIF4AI
α-eIF4E
Endogenous eIF4A
Endogenous eIF4E

Fig. 4